

Journal Pre-proof

Synthesis, spectroscopic characterizations, DFT, molecular docking and molecular dynamics simulations of a novel 2-methyl-3*H*-benzimidazolo[1,2-*b*][1,2,4]triazepin-4(5*H*)-one

Youness El Bakri, El Hassane Anouar, Karthikeyan Subramani, Ali Ben-Yahya, El Mokhtar Essassi

PII: S0022-2860(19)31426-7

DOI: <https://doi.org/10.1016/j.molstruc.2019.127317>

Reference: MOLSTR 127317

To appear in: *Journal of Molecular Structure*

Received Date: 22 September 2019

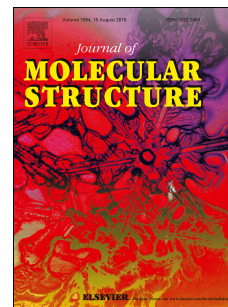
Revised Date: 27 October 2019

Accepted Date: 29 October 2019

Please cite this article as: Y. El Bakri, E.H. Anouar, K. Subramani, A. Ben-Yahya, E.M. Essassi, Synthesis, spectroscopic characterizations, DFT, molecular docking and molecular dynamics simulations of a novel 2-methyl-3*H*-benzimidazolo[1,2-*b*][1,2,4]triazepin-4(5*H*)-one, *Journal of Molecular Structure* (2019), doi: <https://doi.org/10.1016/j.molstruc.2019.127317>.

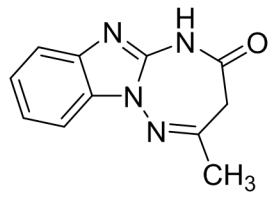
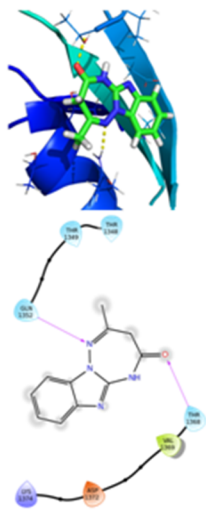
This is a PDF file of an article that has undergone enhancements after acceptance, such as the addition of a cover page and metadata, and formatting for readability, but it is not yet the definitive version of record. This version will undergo additional copyediting, typesetting and review before it is published in its final form, but we are providing this version to give early visibility of the article. Please note that, during the production process, errors may be discovered which could affect the content, and all legal disclaimers that apply to the journal pertain.

© 2019 Published by Elsevier B.V.

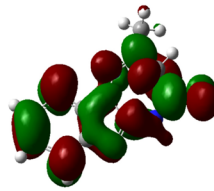




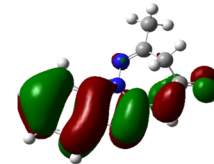
Molecular docking



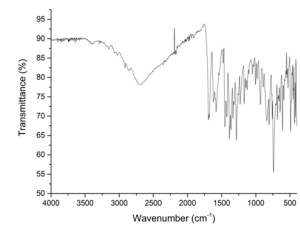
2D chemical structure



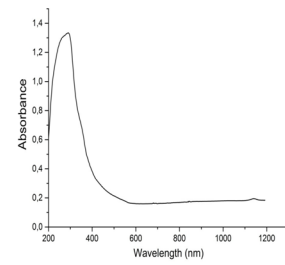
LUMO



HOMO



IR



UV-Vis

Synthesis, spectroscopic characterizations, DFT, Molecular docking and Molecular dynamics simulations of a novel 2-methyl-3*H*-benzimidazolo[1,2-*b*][1,2,4]triazepin-4(5*H*)-one

Youness El Bakri,^{a,b,*} El Hassane Anouar,^{c,*} Subramani Karthikeyan,^b Ali Ben-Yahya,^a and El Mokhtar Essassi^a

^aLaboratoire de Chimie Organique Heterocyclique, URAC 21, Pôle de Compétences Pharmacochimie, Université Mohammed V, Faculté des Sciences, Av. IbnBattouta, BP 1014 Rabat, Maroc.

^bOrganic Chemistry Department, Science Faculty, RUDN University Miklukho-Maklaya st. 6, 117198 Moscow, Russian Federation.

^cDepartment of Chemistry, College of Science and Humanities in Al-Kharj, Prince Sattam bin Abdulaziz University, Al-Kharj 11942, Saudi Arabia.

Corresponding authors

Dr. Youness El Bakri

Tel: +212677288857 Tel: +212677288857 / +79773560777

E-mail address: yns.elbakri@gmail.com

Dr. El Hassane ANOUAR

Tel: +966537237912

E-mail: anouarelhassane@yahoo.fr

Abstract

A novel compound named 2-methyl-3*H*-benzimidazo[1,2-*b*][1,2,4]triazepin-4(5*H*)-one (C₁₁H₁₀N₄O) has been synthesized and characterized by spectroscopic techniques (FT-IR), UV-Vis, ¹H-NMR, ¹³C-NMR and mass spectra. The optimized molecular structure analyses, vibrational wave numbers, ¹³C and ¹H NMR chemical shifts of the title molecule have been performed at DFT/B3LYP method with 6-31+G(d,p) basis set. The electronic absorption wavelengths computed using B3LYP, B3P86 and PBE0 hybrid functional. The scaled vibrational modes, and the predicted ¹³C-NMR and ¹H-NMR chemical shifts are relatively in good agreement with the corresponding experimental ones. However, B3LYP, B3P86 and PBE0 hybrid functional fail in reproduction of experimental λ_{MAX} of the titled compound and it is underestimated by the tested hybrid functionals with deviations to the experimental values of 30, 34 and 40 nm for B3LYP, B3P86 and PBE0, respectively. In addition, molecular docking and molecular dynamics simulations of titled compound were carried out to determine its binding modes and stability within the leucine-rich repeat kinase 2 active site.

Keywords: 1,2-diamino-1*H*-benzimidazole, 1,2,4-triazepine, DFT calculations, Molecular docking, Molecular dynamics

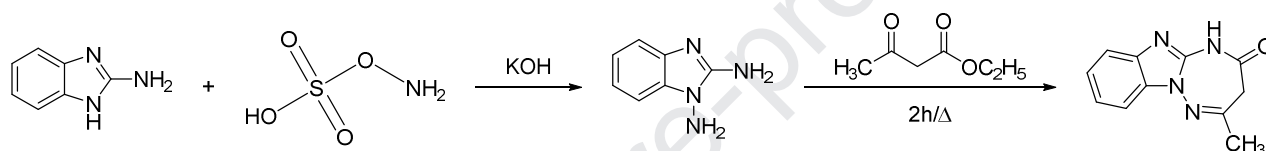
1. Introduction

New synthetic methods continue to be developed to construct seven-membered heterocyclic compounds containing one, two, or three of the heteroatoms N, O, or S. The focus of much of the literature has been non aromatic systems containing at least 1 N atom and has often been driven by a desire to prepare these heterocycles in a stereocontrolled fashion, the search for new bioactives, and the synthesis of natural products. Prominent synthetic methods include transition metal-catalyzed, cycloaddition/annulation, cascade-type, and C-H functionalization processes. Review articles on the synthesis of seven-membered nitrogen heterocycles through the Ugi multicomponent reaction [1], synthetic approaches, and biological activities of benzodiazepines [2], the isolation, structure determination, medicinal properties, and total synthesis of marine natural products containing an oxepanyl ring [3], the synthesis and medicinal importance of benzoxepines [4], methods for the synthesis of 1,2,3-, 1,2,4-, 1,2,5-, and 1,3,5-triazepines [5], and the isolation, biosynthesis, and biological activity of natural products that contain a seven-membered ring with three or more heteroatoms [6] as well as indole-fused azepines and analogs as anticancer lead molecules [7] have been published.

All the heterocyclic compounds are of great interest in pharmaceutical chemistry. Out of these heterocyclic compounds the benzofused heterocyclic compound, i.e. benzimidazole and its derivatives have wide variety of biological activities like antimicrobial activity [8-12], anti-inflammatory-analgesic [13-15], anticancer [16], CNS depressant [17], androgen receptor antagonist [18], antitubercular [19, 20] and anticonvulsant [21-25]. In addition the benzimidazole have played a very important role in the development of theory in heterocyclic chemistry and also extensively in organic synthesis. Due to its wide biological interest we have performed Structural Activity Relationship (SAR) studies for the above titled compound and we found that which is majorly active in kinase family. Based on Swiss target search we

have found leucine-rich repeat kinase 2 (LRRK2) target and this structure from ROC domain from the Parkinson's disease-associated and which reveals a dimericGTPase [26].

As an extension of our research efforts on the design and synthesis of new heterocyclic systems with potent pharmacological properties on 1,2,4-triazole, benzimidazole and 1,2,4-triazepine derivatives [27-30], we describe in the present paper the synthesis, spectroscopic characterizations and computational studies of 2-methyl-3*H*-benzimidazo[1,2-*b*][1,2,4]triazepin-4(5*H*)-one obtained by condensation reaction of 1,2-diamino-1*H*-benzimidazole and ethylacetoacetate (Scheme 1).



Scheme 1. Schematic representation of synthesis of the title compound.

2. Experimental and Theoretical Methods

2.1. Synthesis

A mixture of 1,2-diamino-1*H*-benzimidazole (1 g, 6.75 mmol) and ethyl acetoacetate (4.26mL, 33.78mmol) was heated to 453 K in solvent-free conditions until completion (TLC). The solid product that precipitated was collected by filtration, washed with ethanol.

The FT-IR spectrum of the tilted compound (Figure S1) was recorded directly without dilution in KBr pellets using JASCO FTIR-4160 spectrometer in the range of 4000 – 400 cm^{-1} at resolution of $\pm 2 \text{ cm}^{-1}$. The UV/vis spectrum of the tilted compound (Figure S1) was recorded on a JASCO V-670 spectrophotometer with a simple monochromator for more energy. Our spectrophotometer has the option to cover a spectral range from 190 to 3200 nm. The NMR spectra were measured on a Bruker Avance DPX300 instrument. The chemical shifts (δ) of the tilted compound are expressed in ppm down field from TMS as an internal reference (Figure S3 and S4). Mass spectra (Figure 1) were performed on a Perkin-Elmer

SCIEX API unit 300. The samples are ionized by the ion spray technique (IS). Elemental analysis was performed on a Euro EA - CHNSO Elemental Analyzer. TLC and column chromatography were carried out, respectively, on silica plates (Merck 60 F254) and silica gel (Merck 60, 230-400 mesh).

Yield: 50% mp: 290-293°C IR (ν_{\max} , cm^{-1}): 3517(N-H), 3122(C-H, aromatic), 1648(C=O), 1604(C=N), 1437(C-H, CH_3), 1371(C=C, aromatic). UV ($\lambda_{\max} = 292\text{nm}$). ^1H NMR 300 MHz, (DMSO- d_6), δ (ppm): 2.28 (s, 3H, CH_3), 3.55 (s, 2H, CH_2), 8.71 (s, 1H, NH). ^{13}C NMR 75 MHz, (DMSO- d_6) δ (ppm): δ 24.94, 42.8437, 141.42, 144.08, 164.78, 168.99. HRMS (IE) Calculated for $\text{C}_{11}\text{H}_{10}\text{N}_4\text{O}$: $[\text{M}+\text{H}^+]=214.2310$, Found: $[\text{M}+\text{H}^+]=214.1911$. Elemental analysis Calculated: C, 61.67%; H, 4.71%; N, 26.15%; O, 7.47%, Found: C, 61.70%; H, 4.65%; N, 26.20%; O, 7.45%.

2.2 DFT calculations

Geometry optimization of the ground state (GS) of the tilted compound has been carried out at the DFT level of theory by using the hybrid functionals B3LYP, B3P86 and PBE0 hybrid functionals combined with the double basis set 6-31+G(d,p) as implemented in the Gaussian 16 software package [31]. Polarization and diffuse functions on heavy and hydrogen atoms were added to the double basis set to obtain better accuracy of the results. The ground state minimum for the tilted compound was confirmed by the frequency calculations at the same levels of theory [31]. The calculated vibrational modes were scaled by 0.9679 [32]. The FT-IR and Raman spectra of the tilted compound were calculated using the hybrid functionals B3LYP, B3P86 and PBE0 hybrid functionals combined with the double basis set 6-31+G(d,p) (Figures S5-S7). The predicted ^1H and ^{13}C NMR chemical shifts were obtained within the GIAO approach [33, 34] by calculating the isotropic chemical shielding constants at the same level of theory. The isotropic shielding constants were used to calculate the isotropic chemical shifts, δ_{cal} , with respect to tetramethylsilane (TMS). $\delta_{\text{iso}} = \rho_{\text{TMS}} - \rho_{\text{iso}}$, where δ_{iso} , ρ_{iso} and ρ_{TMS}

are the chemical shift, the absolute shielding and the absolute shielding of TMS, respectively. The solvent effects were taken into account implicitly by using the polarizable continuum model (PCM), for which integral equation formalism is used (IEF-PCM). In the PCM model, the substrate is embedded into a cavity surrounded by a dielectric continuum characterized by its dielectric constant ($\epsilon_{\text{DMSO}} = 46.826$) [35].

2.3 Molecular docking & dynamics studies

The chemical structure of above titled compound was drawn using chem. Draw pro 12 and further energetically minimized using conjugate gradient algorithm using impact panel which is in-built in Schrödinger 2018-2 program. The target molecule of LRRK2 (PDB ID: 2ZEJ) was found based on Swiss target search [36]. The LRRK2 molecule further prepared for using protein preparation wizard for docking studies. The induced fit docking analysis was performed once both small molecule and macromolecule prepared and active site residues were picked up from the co-crystal binding site of LRRK2. Once docking finished, 20 different binding poses were generated and best binding complex were taken based on binding energy and interacting residues for further analysis. For the molecular dynamics studies, best LRRK2 with titled compound was taken and the complex system was built using a periodic boundary condition with a 10 \AA^3 cubic box from the centre of mass of the LRRK2 complex. A TIP3P water solvation system was used in a buffer system with charged ions placed isotropically to neutralise the Ewald charge summation of the solvated LRRK2 complex entity. The system was minimized with maximum iterations of 5000 steps with a gradient convergence threshold of $1.0 \text{ kcal mol}^{-1} \text{ \AA}^{-1}$. Once the system was minimized the system was subjected to Newtonian dynamics of the model system to evaluate energy of the system. A series of 2ps steps was integrated to record the simulation. A six stage NPT ensemble default relaxation process was carried out before performing the molecular dynamics simulation. In the first stage a solute-restrained Brownian dynamics of the ensemble was carried out while

keeping the energy constant using the NVT condition. In the second stage the Berendsen thermostat was used and the NVT (*canonical*) ensemble was allowed to relax with respect to temperature with velocity rescaling of every 1ps applied to non-hydrogen solute sample. Subsequently, the NVT ensemble was changed to an NPT ensemble with a Berendsenbarostat and the system was kept at 1 atm pressure followed by system equilibration of 1ns. Then the ensemble was subjected to a 50 ns molecular dynamics run [37, 38].

3. Results and Discussion

3.1. Mass spectrum

Mass spectrometry (MS) helps identifying the amount and type of fragments present in a sample. Mass spectrum is generally presented as a vertical bar graph, in which each bar represents an ion having a specific mass-to-charge ratio (m/z) and the length of each bar shows the relative abundance of that ion. Most of the ions formed in a mass spectrometer have a single charge; therefore, the m/z value is equivalent to mass itself. The most intense peak is assigned as the base peak corresponding to the abundance of 100%.

In this paper, mass spectrum of the title compound was investigated to analyze possible ionic fragmentations and their stabilities. The experimental mass spectrum of the title molecule is given in Figure 1. The possible fragments were identified by their mass-to-charge ratio (m/z).

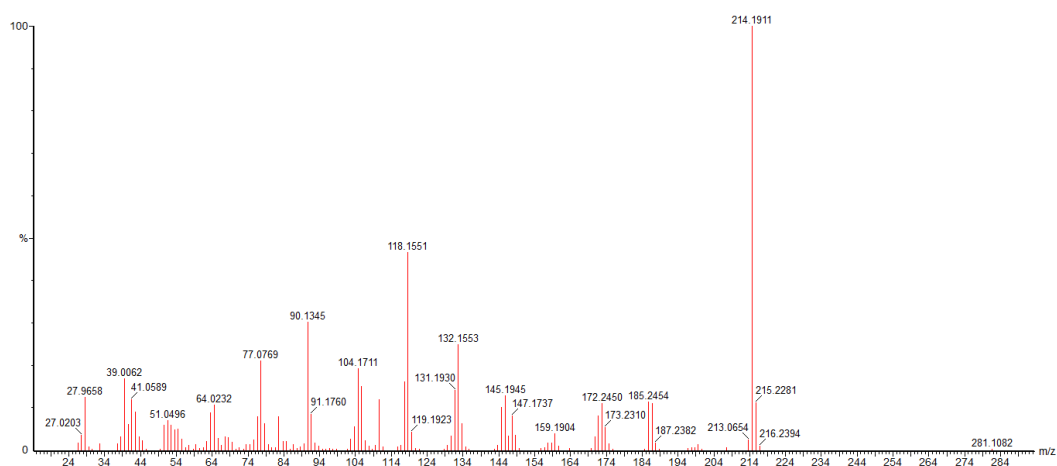
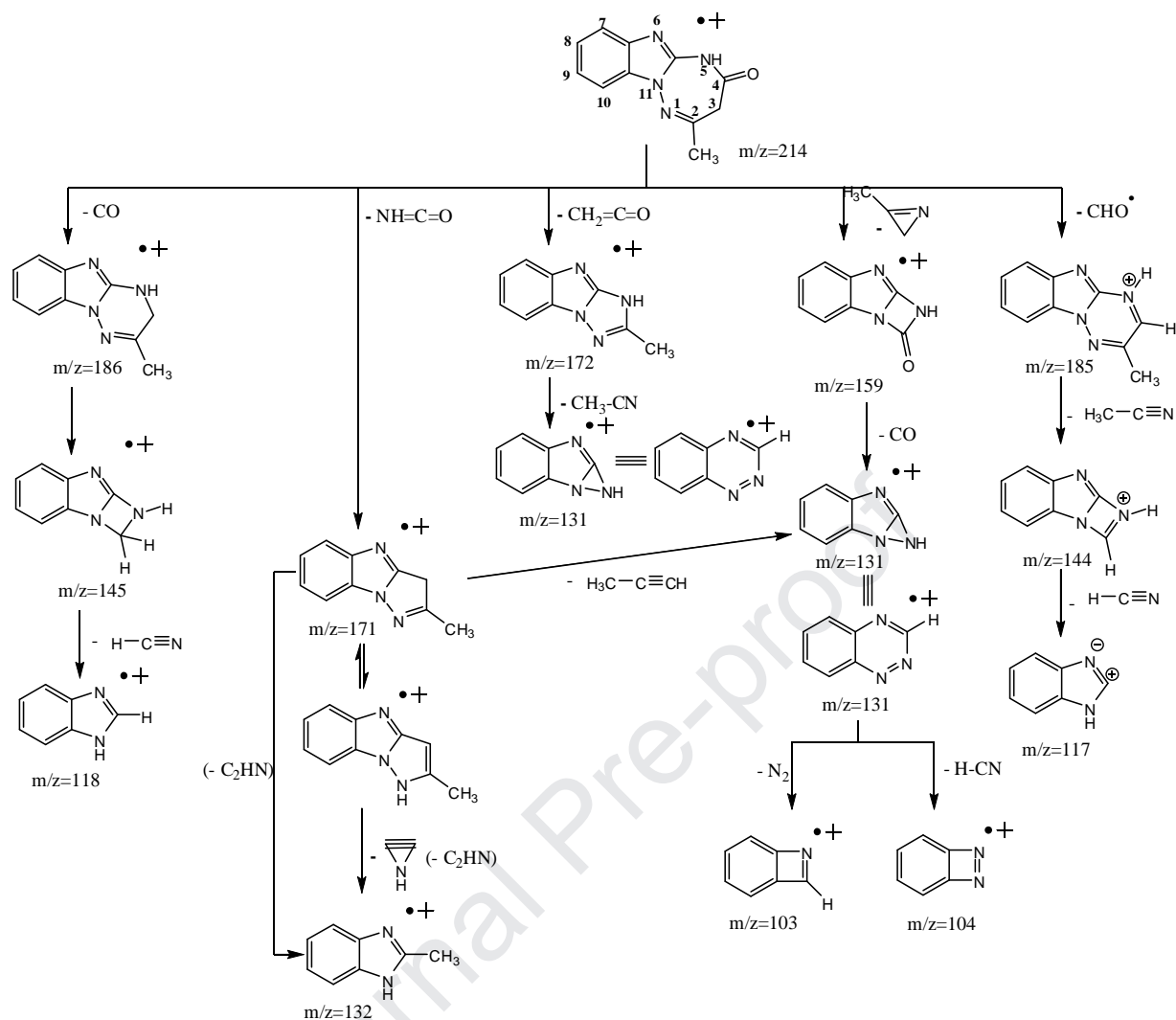


Fig. 1. Mass spectrum of the title compound

The structure of the title compound was also confirmed on the basis of a study in mass spectrometry, using as ionization mode: the electronic impact (**scheme 2**).



Scheme 2. Proposed fragmentation pathway of the title compound.

The molecular ion undergoes mainly five fragmentations:

1-Loss of a ketene molecule to lead to an ion $m/z = 172$ corresponding to a triazolobenzimidazolium structure. This fragmentation is characteristic of the seven-membered compounds having a $-\text{CH}_2-\text{C}=\text{O}$ moiety.

2-Elimination of a carbon monoxide molecule giving rise to an ion at $m/z = 186$ which loses a molecule of acetonitrile to give an ion at $m/z = 145$. The latter undergoes a rearrangement after loss of a molecule of hydrocyanic acid to lead to the benzimidazolium ion at $m/z = 118$

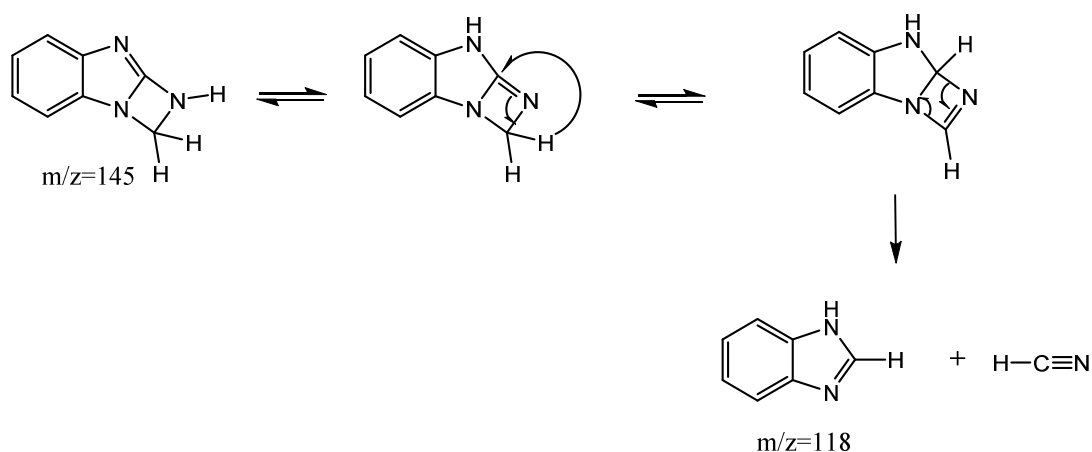
3-Ejection of a molecule of 3-methyl-2*H*-azirine after disruption of the N₁-N₁₁ and C₃-C₄ bonds of the tricyclic system, leading to the ion at $m/z = 159$ of diazetobenzimidazolium structure which loses a molecule of carbon monoxide to lead to the ion at $m/z = 131$.

4-Loss of a radical CHO, giving rise to an ion with $m/z = 185$ of structure triazinobenzimidazolium which loses a molecule of acetonitrile to give an ion at $m/z = 144$ of structure diazetobenzimidazolium which loses a molecule of hydrogen cyanide to give the benzimidazolium ion at $m/z = 117$.

5-Elimination of an isocyanic acid molecule creating an ion at $m/z = 171$ of pyrazolobenzimidazolium structure likely to be in two tautomeric forms. The latter loses a molecule of propyne to lead to an ion at $m/z = 131$ which can be in the form of two isomeric structures: diaziridinobenzimidazolium or benzotriazinium. The latter, more stable ejects a molecule of nitrogen and a molecule of hydrogen cyanide to lead respectively to the ions at $m/z = 103$ and $m/z = 104$.

It should be noted that the ion at $m/z = 131$ can also come from the ion at $m/z = 172$, after loss of a molecule of acetonitrile. Similarly, the losses of CO, CHO and an isocyanic acid molecule make it possible to show the presence, in the molecule studied, of the lactam function.

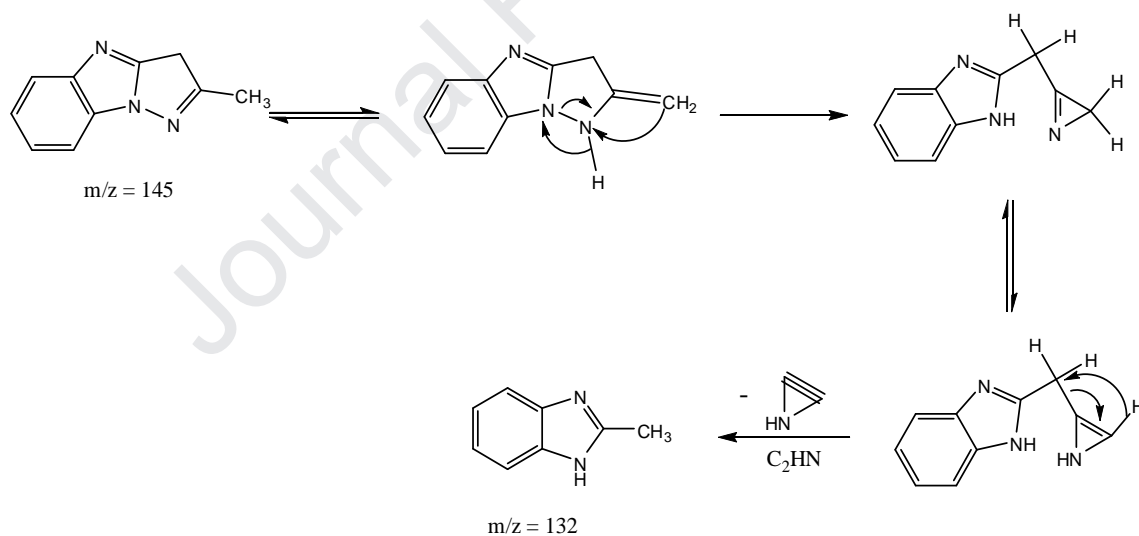
A mechanism can be proposed to explain the formation of the benzimidazolium ion at $m/z = 118$, from the ion at $m/z = 145$ (**scheme 3**).



Scheme 3. Plausible mechanism for the formation of benzimidazolium ion.

The ion at $m/z = 171$ can also lose a molecule of formula C_2HN to give the ion at $m/z = 132$ of 2-methyl-benzimidazolium structure. A mechanism for forming this ion is shown in

Scheme 4.



Scheme 4. Mechanism for the formation of 2-methyl-benzimidazolium.

3.2. ^1H -NMR and ^{13}C -NMR spectra

The experimental and predicted ^1H and ^{13}C NMR chemical shifts for the titled compound are shown in Table 1. Relatively good correlations were obtained between the predicted and experimental chemical shifts of titled compound, with the correlation

coefficients of 99.89 and 99.1% for ^1H -NMR and ^{13}C NMR, respectively (Figure 2). Mean average deviations for ^1H NMR and ^{13}C NMR are 0.11 and 4.37 ppm, respectively. For ^{13}C NMR, the minimal deviation is obtained for the reproduction of the chemical shift of methyl group with a deviation of 1.29 ppm, while the maximal deviation is obtained for $-\text{CH}-$ functional with a deviation of 12.24 ppm. For ^1H NMR, the minimal deviation is obtained for the reproduction of the chemical shift of amine group ($-\text{NH}-$) with a deviation of 0.02 ppm, while the maximal deviation is obtained for $-\text{CH}_2-$ protons with a deviation of 0.12 ppm.

Table 1. Experimental and predicted ^1H and ^{13}C NMR chemical shifts (ppm) for the tilted compound.

^1H -NMR	Predicted	Experimental
(CH ₃ , s, 3H ₃)	2.38	2.28
(CH ₂ , s, 2H ₂)	3.43	3.55
(NH, s, 1H)	8.73	8.71
MAE	0.11	
Max. Dev.	0.12	
Min. Dev.	0.02	
^{13}C -NMR		
(CH ₃)	26.23	24.94
(-CH ₂ -)	44.65	42.84
(-CH-)	129.18	141.42
(C=N)	148.02	144.08
CH ₃ -(C=N)	167.34	164.78
(C=O)	171.66	168.99
(CH ₃)	26.23	24.94
(-CH ₂ -)	44.65	42.84
(-CH-)	129.18	141.42
(-CH-)	148.02	144.08
MAE	4.37	
Max. Dev.	12.24	
Min. Dev.	1.29	

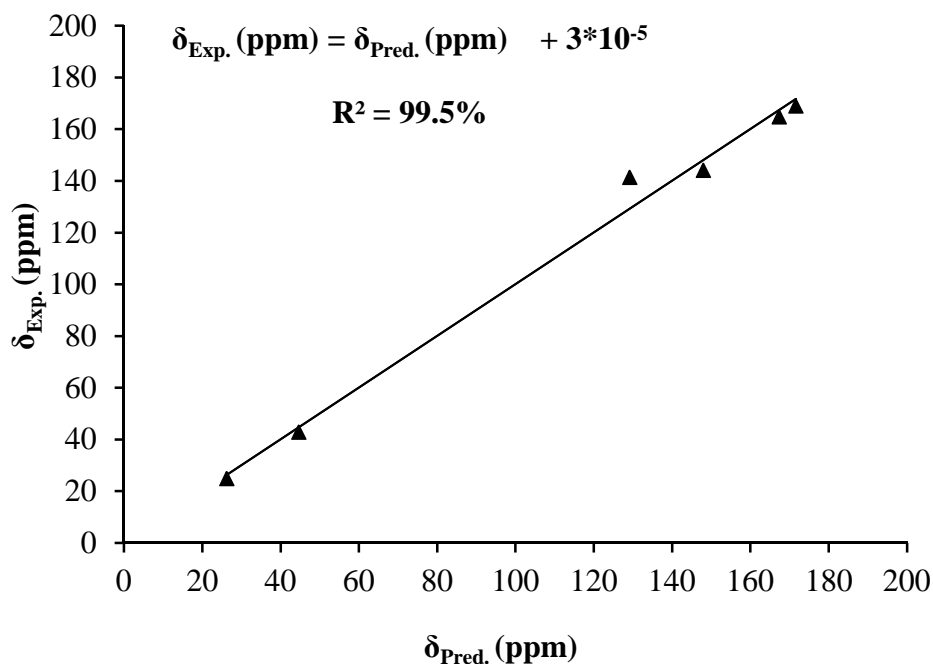


Fig. 2. Correlation curve between the predicted and experimental ^{13}C NMR chemical shifts of the tilted compound.

3.3. Vibration Spectrum

Some of the main experimental, calculated and scaled vibrations modes of the tilted compound, and their corresponding calculated intensities and Raman scattering activities are given in Table 2. The calculated vibration modes are scaled with a factor of 0.9613. The reproduction of the experimental vibration modes depends on the type of vibration mode itself and the hybrid functional used. Mean average deviations, maximal and minimal deviations obtained using with the tested functional are shown in Table 2. Accordingly, the best reproduction is obtained with B3LYP with an MAE of 30 cm^{-1} . For this functional, the lowest deviation is obtained for $\nu\text{C-H}$ (CH_3) with a deviation of 4 cm^{-1} with respect to the observed value. All the tested hybrid functional fail in the reproduction of $\nu\text{C=O}$ with lowest maximal deviation obtained with B3LYP of 80 cm^{-1} . As can be seen in Table 2, the correction of the calculated vibration is improved the reproduction of the experimental values. For instance, the deviation of $\nu\text{C-H}$ (ar) obtained with B3LYP functional before and after

correction are of 99 and 4 cm^{-1} with respect to the experimental value. The root-mean-square deviation (RMS) between the calculated and scaled vibration modes and the observed ones were determined for each tested hybrid functional (Table 2). The lowest RMS value is obtained with B3LYP of 35 cm^{-1} .

Table 2. Calculated and experimental vibrational modes of the tilted compound.

	Calc.	Scal.	I ^{IR}	RA*	Exp
B3LYP					
$\nu_{\text{N-H}}$	3597	3482	72.44	127.11	3523
$\nu_{\text{C-H}}$ (ar)	3221	3118	5.67	168.86	3123
$\nu_{\text{C=O}}$	1785	1728	721.03	79.84	1770
$\nu_{\text{C=N}}$ (C=C)	1695	1640	29.65	145.03	1676
$\nu_{\text{C-H}}$ (CH ₃)	1483	1432	6.59	13.2	1429
$\nu_{\text{C=C}}$ (ar)	1394	1349	1.62	22.1	1378
MAE	30	30	-	-	-
Max. Dev.	137	80	-	-	-
Min. Dev.	23	4	-	-	-
RMS	35	35	-	-	-
B3P86					
$\nu_{\text{N-H}}$	3621	3505	78.25	125.98	3517
$\nu_{\text{C-H}}$ (ar)	3217	3114	11.31	170.06	3122
$\nu_{\text{C=O}}$	1813	1755	722.61	74.64	1648
$\nu_{\text{C=N}}$ (C=C)	1715	1660	26.54	149.87	1604
$\nu_{\text{C-H}}$ (CH ₃)	1476	1429	6.98	15.35	1437
$\nu_{\text{C=C}}$ (ar)	1417	1372	10.35	10.23	1371
MAE	34	32	-	-	-
Max. Dev.	165	107	-	-	-
Min. Dev.	39	1	-	-	-
RMS	41	41	-	-	-
PBE0					
$\nu_{\text{N-H}}$	3640	3523	81.57	122.00	3517
$\nu_{\text{C-H}}$ (ar)	3227	3123	9.96	164.31	3122
$\nu_{\text{C=O}}$	1829	1770	729.9	72.22	1648
$\nu_{\text{C=N}}$ (1,2,4-triazepine)	1732	1676	27.95	152.62	1604
$\nu_{\text{C-H}}$ (CH ₃)	1476	1429	5.36	19.72	1437
$\nu_{\text{C=C}}$ (arc)	1424	1378	5.46	5.70	1371
MAE	39	36	-	-	-
Max. Dev.	181	122	-	-	-
Min. Dev.	39	1	-	-	-
RMS	46	46	-	-	-

* Raman scattering activity

3.4. Electronic absorption spectrum

The experimental and calculated maximum absorption bands of the tilted compound are shown in Table 3. The calculated maximum absorption bands were obtained using B3LYP, B3P86 and PBE0 in gas and IEF-PCM phases. The experimental absorption band at 292 nm corresponds to $\pi \rightarrow \pi^*$ electronic transition. As can be seen from Table 3, the reproduction of λ_{MAX} may depend on the type of the hybrid functional, and the media. In gas phase, the experimental λ_{MAX} of the tilted compound is underestimated by tested hybrid functional with deviation with respect to the experimental of 30, 34 and 40 nm for B3LYP, B3P86 and PBE0, respectively. The solvent has no effect on the position of the absorption bands (Table 3). However, λ_{MAX} is strongly affected in PCM. The solvent-solute interaction induces an hyperchromic shift, *i.e.*, an increase in the absorption intensity. The absorption λ_{MAX} is attributed to H \rightarrow L+1 electronic transition in gas phase, and to H-1 \rightarrow L electronic transition (Figure 3).

Table 3. λ_{MAX} (nm), E_{MAX} (eV), electronic Transition (ET) and oscillator strength (f) of maximum absorption band of the titled compound. The calculations are performed using B3LYP, B3P86 and PBE0 hybrid functional in gas and IEF-PCM phases.

	Calculated				Experimental	
	λ_{MAX}	E_{MAX}	ET	f	λ_{MAX}	E_{MAX}
Gas						
B3LYP	262	4.74	H \rightarrow L+1	0.61		
B3P86	258	4.81	H \rightarrow L+1	0.37		
PBE0	252	4.92	H \rightarrow L+1	0.85		
IEF-PCM					292	4.26
B3LYP	261	4.75	H-1 \rightarrow L	0.66		
B3P86	258	4.81	H-1 \rightarrow L	0.67		
PBE0	251	4.93	H-1 \rightarrow L	0.66		

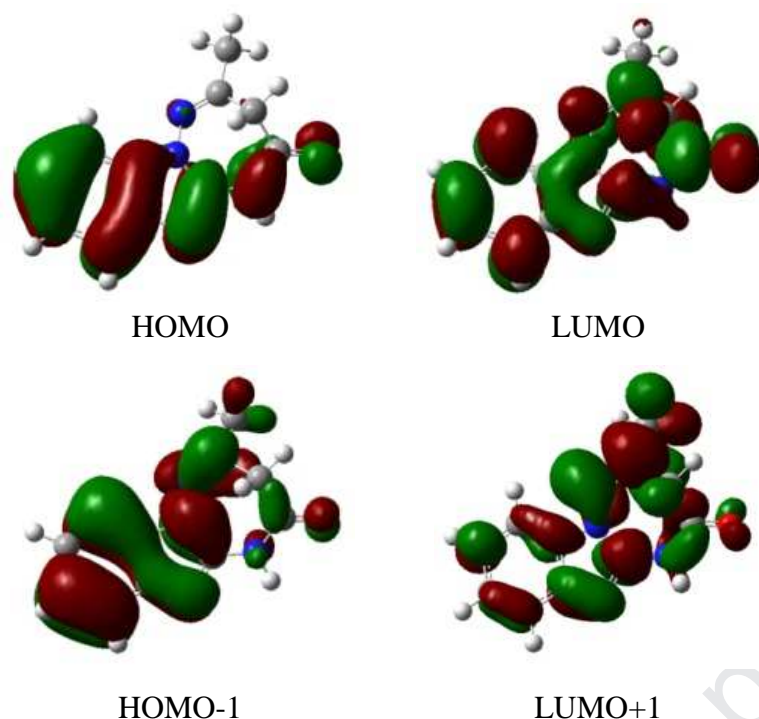


Fig. 3. Molecular orbitals correspond to λ_{MAX} electronic absorption.

3.5. Molecular docking & dynamics analysis

The docking and dynamics studies reveal the information about the binding interaction mechanism between titled compound and LRRK2 (Figure 4). The binding energy for LRRK2–compound complex is -25.45 kcal/mol and which shows the good binding affinity between compound and LRRK2. From the Figure 4c the ligand plot, two hydrogen bonding formation between residues GLN 1352 bonded with N atom and THR 1368 bonded with O atom of titled compound. Also, ASP 1372 and LYS 1374 residues were contact with negatively and positively charged in titled compound binding environment. Mostly polar residues THR 1368, THR 1348, THR 1349 and GLN 1352 were in contact with the titled compound molecule binding environment and VAL 1369 is only having hydrophobic contact with titled compound. The molecular dynamics simulations were carried for to understand the stability of LRRK2- titled compound complex system during 50 ns simulation time The docking and dynamics studies reveal the information about the binding interaction mechanism between

titled compound and LRRK2 (Figure 4). The binding energy for LRRK2 –compound complex is -25.45 kcal/mol and which shows the good binding affinity between compound and LRRK2. From the Figure 2c the ligand plot, two hydrogen bonding formation between residues GLN 1352 bonded with N atom and THR 1368 bonded with O atom of titled compound. Also, ASP 1372 and LYS 1374 residues were contact with negatively and positively charged in titled compound binding environment. Mostly polar residues THR 1368, THR 1348, THR 1349 and GLN 1352 were in contact with the titled compound molecule binding environment and VAL 1369 is only having hydrophobic contact with titled compound. The molecular dynamics simulations were carried for to understand the stability of LRRK2- titled compound complex system during 50 ns simulation time.

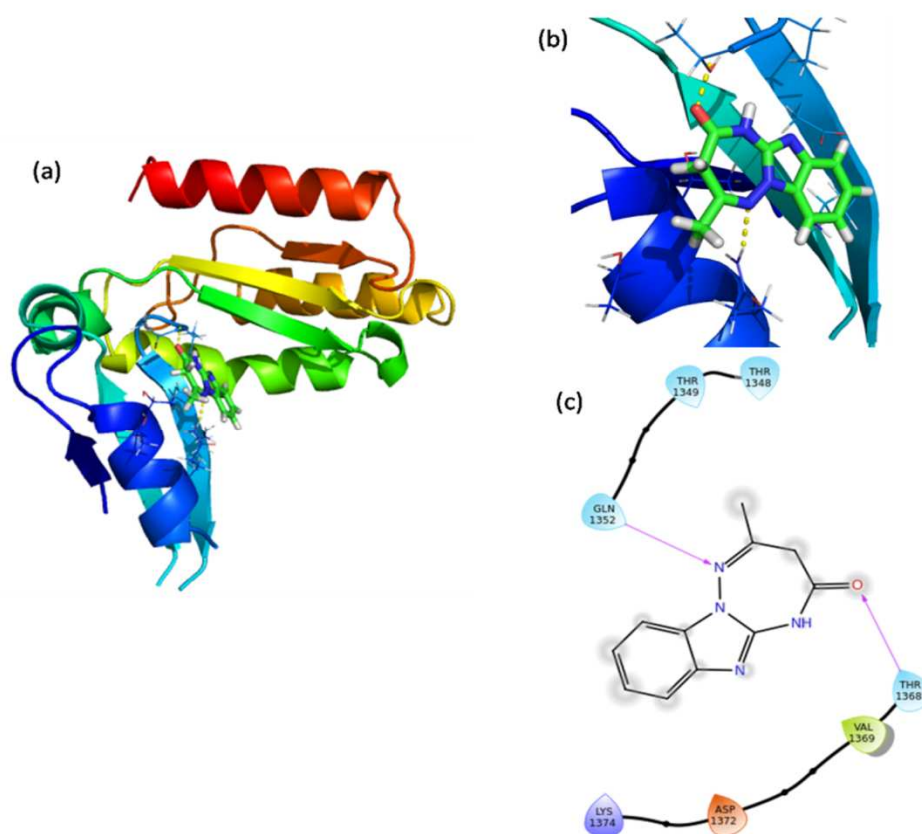


Fig. 4. (a) Best binding pose of titled compound with LRRK2 (b) Ligand plot for LRRK2 – titled compound complex.

As shown in the Figures 5a and 5b Root Mean Square Deviation (RMSD), Root Mean Square Fluctuation (RMSF) analysis will help to understand the LRRK2 – titled compound complex system equilibration and fluctuation throughout the end of simulation time. In Figure 5a RMSD result shows that LRRK2 –titled compound are converged at greater than 3Å, which means the system has large conformation rather than small or globular protein and ligand RMSD (Lig fit Protein) was stable during the throughout the simulation time. In Figures 5b RMSF plot will help to understand local changes of LRRK2 along with protein chain and the green color lines were titled compound binding site residues of LRRK2 during the simulation.

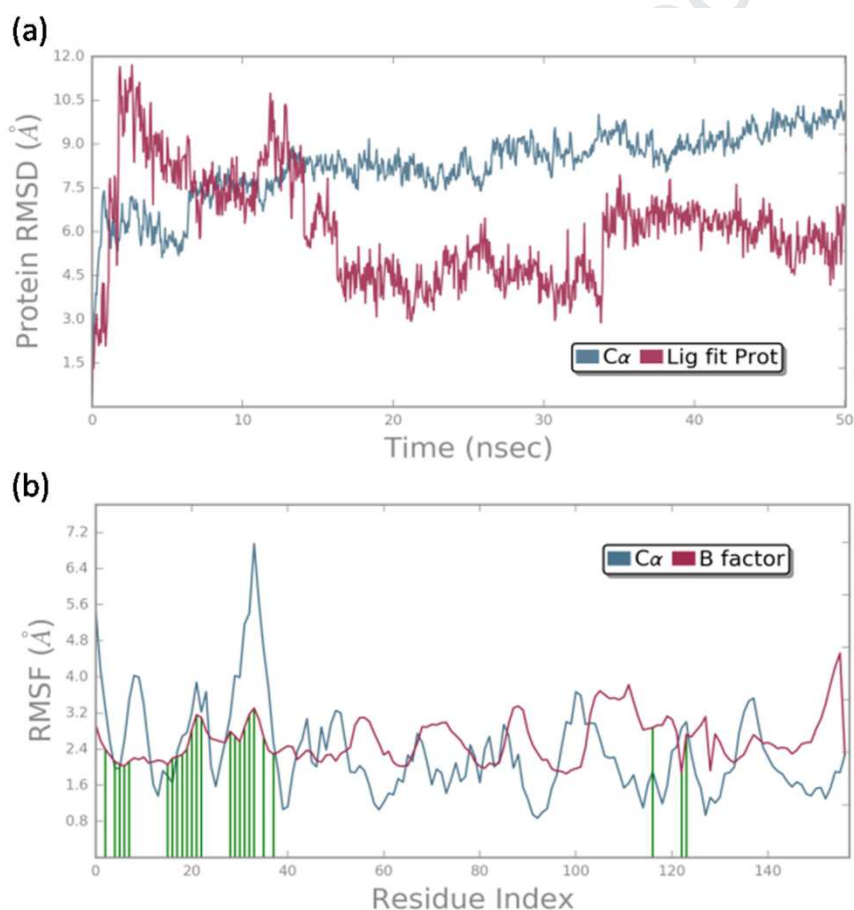


Fig. 5. (a) RMSD (b) RMSF plot of LRRK2 – titled compound complex.

Figures 6a and 6b shows the final molecular dynamics output of LRRK2 – titled compound complex. From that Figure 6a TRP 1376 alone participating above 50 % and remaining residues were contributes below 50 % hydrophobic force with titled compound and

Figure 6b clearly shows that most of the residues were in the form of hydrophobic after molecular dynamics simulation and the overall result concludes that the LRRK2 – titled compound complex system was stable during the 50 ns simulation [39, 40].

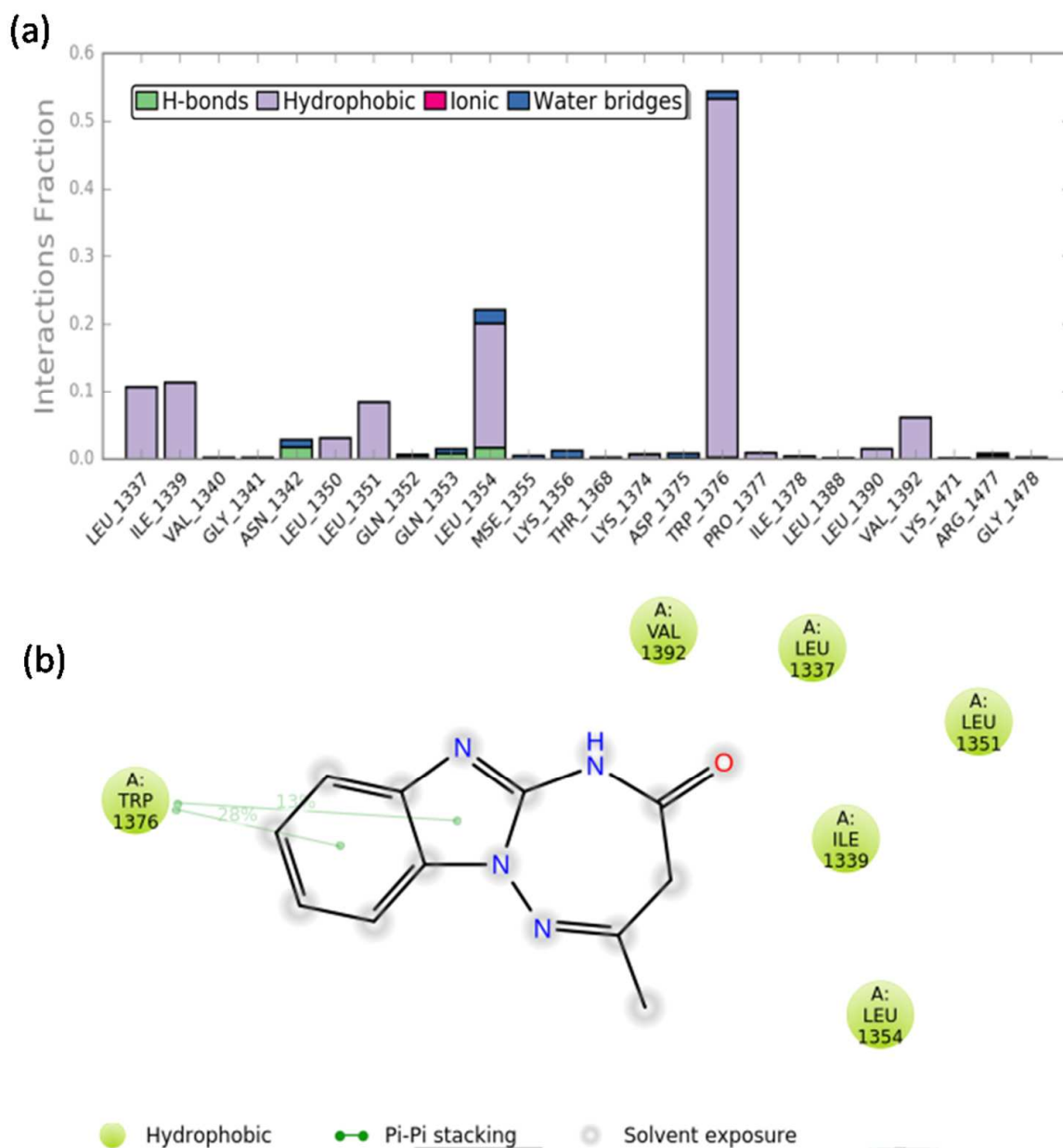


Fig. 6. (a) interaction fraction plot (b) detailed ligand interaction contact of LRRK2 – titled compound complex.

Conclusions

We have reported herein the synthesis of 2-methyl-3*H*-benzimidazolo[1,2-*b*][1,2,4]triazepin-4(5*H*)-one. We have fully characterized them using FT-IR spectroscopies, UV-Vis, MS and NMR (¹H, ¹³C). Subsequently, the optimized structure of the molecule was determined based on DFT calculations by the B3LYP method using Gaussian 16 software package. Molecular docking result concludes that there was good binding affinity between LRRK2 – titled compound and molecular dynamics result suggest that LRRK2 – titled compound complex system was stable during 50 ns simulation time.

Acknowledgements

The publication was prepared with the support of the “RUDN University Program 5-100”.

References

- [1] L. Banfi, A. Basso, C. Lambruschini, L. Moni, R. Riva, Synthesis of seven-membered nitrogen heterocycles through the Ugi multicomponent reaction, *Chem. Heterocycl. Compd.* 53 (2017) 382-408.
- [2] X. Zhao, J. Zhang, Z. Zheng, R. Xu, Facile Synthesis for Benzo-1, 4-Oxazepine Derivatives by Tandem Transformation of CN Coupling/CH Carbonylation, *Molecules* 22 (2016) 53.
- [3] H. Barbero, C. Díez-Poza, A. Barbero, The Oxepane Motif in Marine Drugs, *Mar. Drugs* 15 (2017) 1-34.
- [4] N. Kuntala, J.R. Telu, J.S. Anireddy, S. Pal, A brief overview on chemistry and biology of benzoxepine, *Lett. Drug Des. Discov.* 14 (2017) 1086-1098.
- [5] M. Mohammadi Zeydi, N.O. Mahmoodi, Overview on Developed Synthesis Methods of Triazepane Heterocycles, *J. Chin. Chem. Soc.* 64 (2017) 1023-1034.
- [6] E.K. Davison, J. Sperry, Natural products with heteroatom-rich ring systems, *J. Nat. Prod.* 80 (2017) 3060-3079.
- [7] A.K. Singh, V. Raj, S. Saha, Indole-fused azepines and analogues as anticancer lead molecules: Privileged findings and future directions, *Eur. J. Med. Chem.* 142 (2017) 244-265.

- [8] B.V.S. Kumar, S.D. Vaidya, R.V. Kumar, S.B. Bhirud, R.B. Mane, Synthesis and antibacterial activity of some novel 2-(6-fluorochroman-2-yl)-1-alkyl/acyl/aroyl-1H-benzimidazoles, *Eur. J. Med. Chem.* 41 (2006) 599-604.
- [9] A.H. El-Masry, H. Fahmy, S. Ali Abdelwahed, Synthesis and antimicrobial activity of some new benzimidazole derivatives, *Molecules* 5 (2000) 1429-1438.
- [10] Z. Kazimierczuk, J. Upcroft, P. Upcroft, A. Gorska, B. Starosciak, A. Laudy, Synthesis and antiprotozoal activity of some 2-(trifluoromethyl)-1H-benzimidazole bioisosteres, *Acta. Biochim. Pol* 49 (2002) 185-195.
- [11] N. Shetgiri, S. Kokitkar, Synthesis and biological activity of new benzimidazoles, *Indian J. Chem.* 40B (2001) 163-166.
- [12] K. Ansari, C. Lal, Synthesis and evaluation of some new benzimidazole derivatives as potential antimicrobial agents, *Eur. J. Med. Chem.* 44 (2009) 2294-2299.
- [13] S.A. Khan, A.M. Nandan, 2-Substituted benzimidazoles as antiinflammatory and analgesic agents, *Indian J. Heterocy. Ch.* 7 (1997) 55-58.
- [14] D. Evans, T. Hicks, W. Williamson, W. Dawson, S. Meacock, E. Kitchen, Synthesis of a group of 1H-benzimidazoles and their screening for antiinflammatory activity, *Eur. J. Med. Chem.* 31 (1996) 635-642.
- [15] M.A. Taha, Synthesis and antiinflammatory evaluation of some imino-sugars of methylbenzimidazole, *J. Indian Chem. Soc.* 82 (2005) 180-182.
- [16] Ş. Demirayak, U.A. Mohsen, A.Ç. Karaburun, Synthesis and anticancer and anti-HIV testing of some pyrazino [1, 2-a] benzimidazole derivatives, *Eur. J. Med. Chem.* 37 (2002) 255-260.
- [17] P. Sharma, A. Mandloi, S. Pritmani, Synthesis of new 2-(substituted benzothiazolylcarbamoyl) benzimidazoles as potential CNS depressants, 38B (1999) 1289-1294.
- [18] R.A. Ng, J. Guan, V.C. Alford Jr, J.C. Lanter, G.F. Allan, T. Sbriscia, O. Linton, S.G. Lundeen, Z. Sui, Synthesis and SAR of potent and selective androgen receptor antagonists: 5, 6-Dichloro-benzimidazole derivatives, *Bioorg. Med. Chem. Lett.* 17 (2007) 784-788.
- [19] P.R. Kagthara, N.S. Shah, R.K. Doshi, H. Parekh, Synthesis of 2, 5-disubstituted 1, 3, 4-oxadiazoles as biologically active heterocycles, 38B (1999) 572-576.
- [20] H. Foks, D. Pancechowska-Ksepko, W. Kuzmierkiewicz, Z. Zwolska, E. Augustynowicz-Kopec, M. Janowiec, Synthesis and tuberculostatic activity of new benzimidazole derivatives, *Chem. Heterocycl. Compd.* 42 (2006) 611-614.

- [21] A. Chimirri, A. De Sarro, G. De Sarro, S. Grasso, G.R. Trimarchi, M. Zappala, Synthesis and anticonvulsant properties of 2, 3, 3a, 4-tetrahydro-1H-pyrrolo [1, 2-a] benzimidazol-1-ones, *J. Med. Chem.* 32 (1989) 93-95.
- [22] A. Chimirri, A. De Sarro, G. De Sarro, R. Gitto, M. Zappala, Synthesis and anticonvulsant properties of 2, 3, 3a, 4-tetrahydro-1H-pyrrolo [1, 2-a] benzimidazol-1-one derivatives, *Il Farmaco* 56 (2001) 821-826.
- [23] L. Vostrova, T. Voronina, T. Karaseva, S. Gernega, É. Ivanov, A. Kirichenko, M.Y. Totrova, Synthesis and anticonvulsant activity of benzimidazo [1, 2-c] quinazolines, *Pharm. Chem. J.* 20 (1986) 404-406.
- [24] J.M. Singh, Possible anticonvulsant thiazolo [3, 2-a] benzimidazole Mannich bases. XI, *J Med. Chem.* 12 (1969) 962-962.
- [25] J.M. Singh, Chemistry of azole derivatives. XII. Possible anticonvulsant thiazolo [3, 2-a] benzimidazoles, *J Med. Chem.* 13 (1970) 1018-1018.
- [26] J. Deng, P.A. Lewis, E. Greggio, E. Sluch, A. Beilina, M.R. Cookson, Structure of the ROC domain from the Parkinson's disease-associated leucine-rich repeat kinase 2 reveals a dimeric GTPase, *Proc. Natl. Acad. Sci.* 105 (2008) 1499-1504.
- [27] Y. El Bakri, E.H. Anouar, I. Marmouzi, K. Sayah, Y. Ramli, M.E.A. Faouzi, E.M. Essassi, J.T. Mague, Potential antidiabetic activity and molecular docking studies of novel synthesized 3,6-dimethyl-5-oxo-pyrido [3, 4-f][1, 2, 4] triazepino [2, 3-a] benzimidazole and 10-amino-2-methyl-4-oxo pyrimido [1, 2-a] benzimidazole derivatives, *J. Mol. Model.* 24 (2018) 1-10.
- [28] Y. El Bakri, L. Guo, E.H. Anouar, A. Harmaoui, A.B. Ali, E.M. Essassi, J.T. Mague, Synthesis, crystal structure, DFT, molecular dynamics simulation and evaluation of the anticorrosion performance of a new pyrazolotriazole derivative, *J. Mol. Struct.* 1176 (2019) 290-297.
- [29] Y. El Bakri, Y. Ramli, E.M. Essassi, J.T. Mague, Synthesis, crystal structure, spectroscopic characterization, Hirshfeld surface analysis, and DFT calculations of 1, 4-dimethyl-2-oxo-pyrimido [1, 2-a] benzimidazole hydrate, *J. Mol. Struct.* 1152 (2018) 154-162.
- [30] Y. El Bakri, C.-H. Lai, J. Sebhaoui, A.B. Ali, Y. Ramli, E.M. Essassi, J.T. Mague, Synthesis, crystal structure, Hirshfeld surface analysis, and DFT calculations of new 1-[(1-benzyl-1H-1, 2, 3-triazol-4-yl) methyl]-6-methoxy-1H-benzimidazol-2 (3H)-one, *CDC* 17 (2018) 472-482.

- [31] M. Frisch, G. Trucks, H. Schlegel, G. Scuseria, M. Robb, J. Cheeseman, G. Scalmani, V. Barone, B. Mennucci, G. Petersson, Gaussian 09, revision D. 01, Gaussian, Inc., Wallingford CT, 2009.
- [32] M. Andersson, P. Uvdal, New scale factors for harmonic vibrational frequencies using the B3LYP density functional method with the triple- ζ basis set 6-311+ G (d, p), *J. Phys. Chem. A* 109 (2005) 2937-2941.
- [33] R. Ditchfield, Molecular orbital theory of magnetic shielding and magnetic susceptibility, *J. Chem. Phys.* 56 (1972) 5688-5691.
- [34] K. Wolinski, J.F. Hinton, P. Pulay, Efficient implementation of the gauge-independent atomic orbital method for NMR chemical shift calculations, *J. Am. Chem. Soc.* 112 (1990) 8251-8260.
- [35] J. Tomasi, B. Mennucci, R. Cammi, Quantum Mechanical Continuum Solvation Models, *Chem. Rev.* 105 (2005) 2999-3093.
- [36] D. Gfeller, O. Michielin, V. Zoete, Shaping the interaction landscape of bioactive molecules, *Bioinformatics* 29 (2013) 3073-3079.
- [37] B.S. Schrödinger, LLC: New York, 2018.
- [38] S. Release, 3: Desmond molecular dynamics system, DE Shaw research, New York, NY, 2017, Maestro-Desmond Interoperability Tools, Schrödinger, New York, NY (2017).
- [39] S. Karthikeyan, G. Bharanidharan, S. Ragavan, S. Kandasamy, S. Chinnathambi, K. Udayakumar, R. Mangaiyarkarasi, A. Sundaramoorthy, P. Aruna, S. Ganesan, Comparative Binding Analysis of N-Acetylneuraminic Acid in Bovine Serum Albumin and Human α -1 Acid Glycoprotein, *J. Chem. Inf. Model.* 59 (2018) 326-338.
- [40] S. Karthikeyan, G. Bharanidharan, S. Ragavan, S. Kandasamy, S. Chinnathambi, K. Udayakumar, R. Mangaiyarkarasi, R. Suganya, P. Aruna, S. Ganesan, Exploring the Binding Interaction Mechanism of Taxol in β -Tubulin and Bovine Serum Albumin: A Biophysical Approach, *Mol. Pharm.* 16 (2019) 669-681.

1. 2-methyl-3*H*-benzimidazolo[1,2-*b*][1,2,4]triazepin-4(5*H*)-one was synthesized and characterized.
2. Molecular structure is characterized by using spectroscopic techniques.
3. DFT calculations at B3LYP allow a better reproduction of the experimental data.
4. Molecular docking and molecular dynamics analysis were carried with leucine-rich repeat kinase 2 complex

Journal Pre-proof

Declaration of interests

The authors declare that they have no known competing financial interests or personal relationships that could have appeared to influence the work reported in this paper.

The authors declare the following financial interests/personal relationships which may be considered as potential competing interests: